Refractive index maps and membrane dynamics of human red blood cells parasitized by *Plasmodium falciparum*

YongKeun Park*†, Monica Diez-Silva†‡, Gabriel Popescu*§, George Lykotrafitis‡, Wonshik Choi*, Michael S. Feld*, and Subra Suresh¶‖

*G. R. Harrison Spectroscopy Laboratory, ‡Department of Materials Science and Engineering, and ¶School of Engineering and Harvard-MIT Division of Health Science and Technology, Massachusetts Institute of Technology, Cambridge, MA 02139

Communicated by Zdeněk P. Bažant, Northwestern University, Evanston, IL, July 25, 2008 (received for review May 18, 2008)

Parasitization by malaria-inducing *Plasmodium falciparum* leads to structural, biochemical, and mechanical modifications to the host red blood cells (RBCs). To study these modifications, we investigate two intrinsic indicators: the refractive index and membrane fluctuations in *P. falciparum*-invaded human RBCs (*Pf*-RBCs). We report experimental connections between these intrinsic indicators and pathological states. By employing two noninvasive optical techniques, tomographic phase microscopy and diffraction phase microscopy, we extract three-dimensional maps of refractive index and nanoscale cell membrane fluctuations in isolated RBCs. Our systematic experiments cover all intraerythrocytic stages of parasite development under physiological and febrile temperatures. These findings offer potential, and sufficiently general, avenues for identifying, through cell membrane dynamics, pathological states that cause or accompany human diseases.

erythrocyte | febrile temperature | malaria | mechanical properties | optical techniques

During the intraerythrocytic development, the malaria parasite *Plasmodium falciparum* causes structural, biochemical, and mechanical changes to host red blood cells (RBCs). Major structural changes include the formation of parasitophorus vacuoles that surround the growing parasite in their host RBCs, loss of cell volume, and the appearance of small, nanoscale protrusions or "knobs," on the membrane surface (1). From the biochemical standpoint, a considerable amount of hemoglobin (Hb) is digested by parasites during intraerythrocytic development and converted into insoluble polymerized forms of heme, known as hemozoin (2, 3). Hemozoin appears as brown crystals in the vacuole of parasite in later maturation stages of *P. falciparum*-invaded human RBCs (*Pf*-RBCs).

Two major mechanical modifications are loss of RBC deformability (4–6) and increased cytoadherence of the invaded RBC membrane to vascular endothelium and other RBCs (7). These changes lead to sequestration of RBCs in microvasculature in the later stages of parasite development, which is linked to vital organ dysfunction in severe malaria. In the earlier stage, where some loss of deformability occurs, *Pf*-RBCs continue to circulate in the bloodstream.

Membrane dynamics of RBCs can be influenced by human disease states. Fluctuations in phospholipid bilayer and attached spectrin network are known to be altered by cytoskeletal defects, stress, and actin-spectrin dissociations arising from metabolic activity linked to adenosine 5′-triphosphate (ATP) concentration (8–12). Proteins transported from invading organisms, such as the virulent malaria-inducing parasite *P. falciparum*, to specific binding sites in the spectrin network are considered to introduce significant alterations to RBC membrane dynamics and mechanical response (13, 14). These changes could provide insights into possible mechanistic pathways in the pathogenesis of malaria, because the parasite alters biophysical properties of RBCs during its intraerythrocyte stage that lasts up to 48 h. Despite the broad realization that membrane fluctuations provide information on critical interactions among subcellular structure, mechanical stress, and biochemical links between the cell interior and the external environment, systematic experiments of cell membrane dynamics, over the physiologically relevant temperature range, have not been performed.

A clinical feature of symptomatic *P. falciparum* malaria is the presence of periodic episodes of high fever. Previous studies report that fever influences *P. falciparum* survival rate and deformability of *Pf*-RBCs (14, 15). Specifically, loss of deformability at ring stage was found to be more severe at febrile temperature (41°C) compared with physiological temperature (37°C). However, *in vitro* experiments at febrile and physiological temperature only reveal a partial story of what is experienced *in vivo*. When physiological temperature is restored after a fever episode, infected RBCs in circulation might not fully recover properties typically observed at physiological temperature. If the changes to deformability observed at fever conditions are irreversible, prior effects of fever on *Pf*-RBCs would remain. As a consequence, *Pf*-RBCs in circulation at physiological temperature may actually display deformability closer to those measured at febrile temperature. To explore this possibility, we measure the deformability of *Pf*-RBCs at physiological temperature after a transient exposure to febrile temperature to simulate the *in vivo* behavior after a febrile episode. When combined with deformability measurements at static physiological and febrile temperatures, these results give useful insights into how *Pf*-RBCs behave *in vivo*.

In this article, we present two intrinsic indicators that quantitatively and noninvasively elucidate the consequences on cell biomechanics of *P. falciparum* malaria: three-dimensional distributions of refractive index and the membrane fluctuations in *Pf*-RBCs. The refractive index maps of *Pf*-RBCs show the morphological alterations of host RBCs and the structures of vacuoles of parasites. In addition, the refractive index is translated into quantitative information about Hb content of individual *Pf*-RBCs. During the intraerythrocytic stages of *P. falciparum*, we show the decrease of both the total amount and the concentration of Hb in the cytoplasm of *Pf*-RBCs. Thermally driven membrane fluctuations in *Pf*-RBCs are strongly correlated with the material properties of cell mem-

Author contributions: Y.P., M.D.-S., G.P., G.L., W.C., M.S.F., and S.S. designed research; Y.P., M.D.-S., and W.C. performed research; G.P., W.C., and M.S.F. contributed new reagents/analytic tools; Y.P., M.D.-S., and G.L. analyzed data; and Y.P., M.D.-S., G.L., W.C., and S.S. wrote the paper.

The authors declare no conflict of interest.

Freely available online through the PNAS open access option.

†These authors contributed equally to this work.

§Present address: Quantitative Light Imaging Laboratory, Department of Electrical and Computer Engineering, Beckman Institute for Advanced Science and Technology, University of Illinois at Urbana-Champaign, Urbana, IL 61801.

‖To whom correspondence should be addressed. E-mail: ssuresh@mit.edu.

This article contains supporting information online at www.pnas.org/cgi/content/full/0806100105/DCSupplemental.

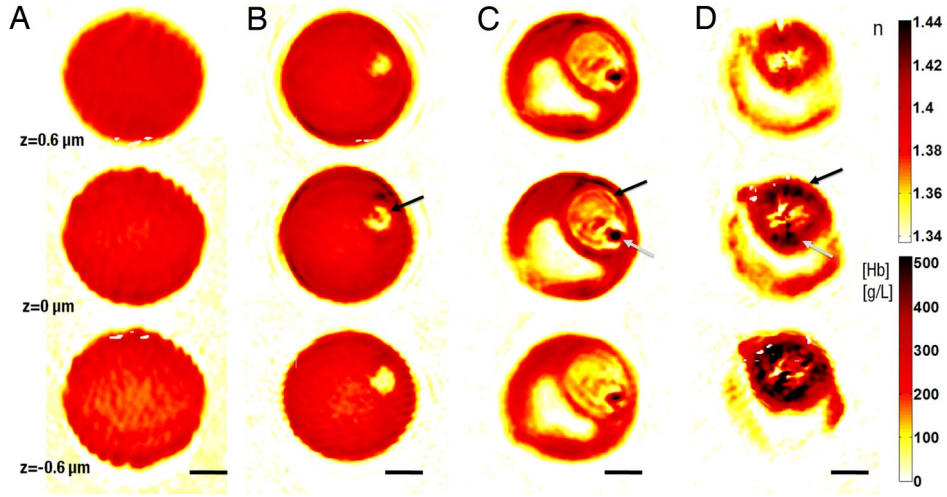

Fig. 1. Three-dimensional refractive index maps of *Pf*-RBCs reveal the structural modifications and the hemoglobin concentration of cytoplasm. (*A*) Healthy RBC. (*B*) Ring stage. (*C*) Trophozoite stage. (*D*) Schizont stage. Images in row show three different cross-sections: 0.6 μm above the focused plane (*Top*), at the focused plane (*Middle*), and 0.6 μm below the focused plane (*Bottom*). Black arrows indicate the location of *P. falciparum*, and the gray arrows the location of hemozoin. Color maps show the refractive index (*n*) (*Top Right*) and the Hb concentration (*Bottom Right*). (Scale bar, 1.5 μm.)

branes, which are significantly modified by the specific proteins exported by parasites during developmental stages. Fluctuations in *Pf*-RBCs membrane are used to characterize the membrane stiffness by determining the in-plane shear modulus. We present experimental results of membrane fluctuations in *Pf*-RBCs over the full range of intraerythrocyte stages at both physiological and febrile temperatures, representative of malaria fever episodes. Parasite interactions with host RBCs strongly correlate with temperature-dependent and stage-specific alterations to membrane dynamics. We critically assess the hypothesis that after exposure to febrile temperature, *Pf*-RBCs at physiological temperature display deformability closer to those at febrile temperature.

Results

Three-dimensional Refractive Index Maps of *Pf*-RBCs. To quantitatively investigate the refractive index distribution of *Pf*-RBCs, we used tomographic phase microscopy (TPM) (16). TPM uses laser interferometry combined with rotating the incident beam, analogous to computed tomography (CT) in x-ray. TPM quantitatively provides the three-dimensional distribution of refractive index, $n(x, y, z)$. As shown in Fig. 1, we measured the refractive index maps of *Pf*-RBCs during all intraerythrocytic stages: healthy RBC (Fig. 1*A*), ring (Fig. 1*B*), trophozoite (Fig. 1*C*), and schizont stage (Fig. 1*D*). Images in the horizontal rows show refractive index maps at three different cross-sections: 0.6 μm above the focused plane (*Top*), at the focused plane (*Middle*), and 0.6 μm below the focused plane (*Bottom*). Whereas healthy RBCs show homogeneous distribution of refractive index, *Pf*-RBCs are not optically homogeneous. Many factors contribute to refractive index change: the vacuole of parasite occupies a fraction of volume in cytoplasm of RBC; Hb is metabolized and converted into hemozoin crystal in the parasite membrane; and various parasite proteins are exported from parasite into cytoplasm of *Pf*-RBCs (17). Regions of low refractive index indicate the vacuole of *P. falciparum* (Fig. 1 *B–D*, black arrows) and regions of high refractive index suggest the position of hemozoin (Fig. 1 *C* and *D*, gray arrows).

Hemoglobin Content in Individual *Pf*-RBCs. To quantitatively investigate the Hb content in *Pf*-RBCs we used refractive index maps measured by TPM. We averaged the refractive index over the cytoplasmic volume of *Pf*-RBC for 15 cells per group (Fig. 2*A*). Their mean values are 1.399 ± 0.006, 1.395 ± 0.005, 1.383 ± 0.005, and 1.373 ± 0.006 for healthy RBCs, ring, trophozoite, and schizont stage, respectively. Given that the cytoplasm of RBCs consists mainly of Hb, it is likely that the refractive index is mostly due to the content of Hb. We calculated Hb concentration for individual *Pf*-RBCs by calibrating from the refractive index of Hb solutions reported in ref. 18. The results are shown in Fig. 2*B*. The mean values of Hb concentration are 30.9 ± 3.1, 29.3 ± 2.4, 23.3 ± 2.7, and 18.7 ± 2.9 g/dl for healthy RBCs, ring, trophozoite, and schizont stage, respectively. Because TPM also provides three-dimensional structural information, we calculated cytoplasmic volume of *Pf*-RBCs by subtracting the volume of parasites vacuole from the volume of whole RBC. The results are shown in Fig. 2*C*. Their mean values are 93.1 ± 7.9, 88.5 ± 11.8, 57.5 ± 13.8, and 34.2 ± 15.1 fl for healthy RBCs, ring, trophozoite, and schizont stage, respectively. In addition, we calculated total Hb contents per each *Pf*-RBC. The total amount of Hb in cytoplasmic volume is given by multiplying Hb concentration and cytoplasmic volume. The results are shown in Fig. 2*D*. Their mean values are 28.8 ± 1.2, 25.9 ± 4.2, 13.4 ± 3.4, and 6.3 ± 2.5 pg for healthy RBCs, ring, trophozoite, and schizont stage, respectively.

Changes in Morphology and Deformability of *Pf*-RBCs During All Intraerythrocytic Stages. To quantify the progressive alterations to RBC membrane fluctuations and mechanical response because of parasitization by *P. falciparum*, we used diffraction phase microscopy (DPM). By extracting optical path-length shifts produced at each point across the cell, DPM quantitatively measures cell thickness information with spatial and temporal resolutions of nanometer and millisecond, respectively (19). This information was then translated into the cell thickness profile, $h(x, y; t)$, by taking into account the optical homogeneity of the internal cell composition along the optical path, which was captured through its refractive index. We used TPM to extract average values of refractive index of cytoplasm of healthy and *Pf*-RBCs. To investigate morphological changes of *Pf*-RBCs, we measured the instantaneous thickness profile, $h(x, y; t_0)$ of cells with DPM (see *Methods*, supporting information (SI) *Text*, Movies S1–S4, and Figs. S1 and S2). Fig. 3 *A–D* shows topographic images of healthy and *Pf*-RBCs at all stages of development. The effective stiffness map of the cell, $k_e(x, y)$, was obtained at each point on the cell, assuming an elastic restoring force associated with the membrane:

$$k_e(x, y) = k_B T / \langle \Delta h(x, y)^2 \rangle,$$

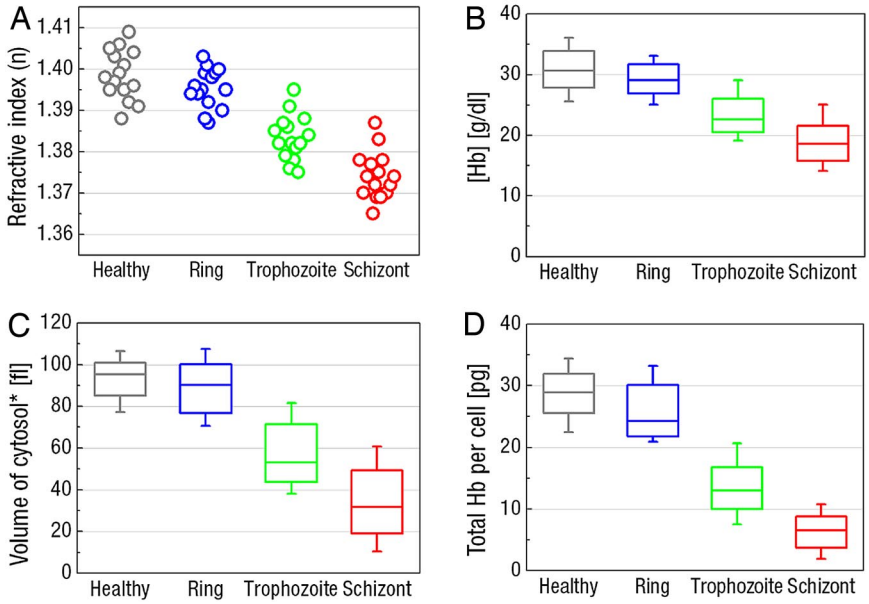

Fig. 2. Host RBC Hb concentrations decreases as *P. falciparum* matures. (*A*) Refractive index of healthy RBC and *Pf*-RBCs at the indicated stages. (*B*) Mean corpuscular Hb concentration (MCHC) of healthy and *Pf-RBCs* at the indicated stages. (*C*) Cytoplasm volume of *Pf-RBCs* at the indicated stages. (*D*) Hb content in healthy and *Pf-RBCs* at the indicated stages. Each point in *A* represents average refractive index for one cell. Graphs in *B–D* show the median (central horizontal line), standard deviations (box), and minimum and maximum values (vertical lines). For each condition, 15 samples were tested.

where k_B is the Boltzmann constant, T is the absolute temperature, and $\langle \Delta h(x, y)^2 \rangle$ the mean-squared displacement. Representative k_e maps of RBCs at the indicated stages of parasite development are shown in Fig. 3 *E–H*. The map of instantaneous displacement of cell membrane fluctuation, $\Delta h(x, y, t)$, was obtained by subtracting time-averaged cell shape from each thickness map in the series. A histogram showing membrane displacements for all parasite stages is shown in Fig. 4*A*.

RBC deformability is sensitive to membrane stiffness. Our DPM experiments provide quantitative information from which in-plane shear modulus of RBC membrane with attached spectrin cytoskeleton could be determined. The in-plane shear modulus G can be obtained by using the Fourier-transformed Hamiltonian (strain energy) and equipartition theorem (20):

$$G \approx \frac{k_B T \ln(A/a)}{3\pi \langle \Delta h_1^2 \rangle},$$

where A is the projected diameter of RBC (≈8 μm), and a is the minimum spatial wavelength measured by DPM (≈0.5 μm). The tangential component of displacement in membrane fluctuations, Δh_t^2 was decoupled from axial membrane fluctuation Δh^2 by using the angle α between the direction of Δh_t and the normal direction of membrane as illustrated in Fig. 4*B Inset*. The angle α was extracted from cell topographical information measured by DPM. Δh_t^2 was calculated and averaged along the circumference of cell, from which in-plane shear modulus G was calculated. We determined that $G = 5.5 \pm 0.8$ μN/m for healthy RBCs (Fig. 4*B*), which compares well with independent modulus measurements, extracted for healthy RBCs from micropipette aspiration and optical tweezers (14, 21, 22). The modulus for ring ($G = 15.3 \pm 5.4$ μN/m), trophozoite ($G = 28.9 \pm 8.2$ μN/m), and schizont ($G = 71.0 \pm 20.2$ μN/m) stages is in good quantitative agreement with that inferred from large-deformation stretching with optical tweezers of *Pf*-RBCs over all stages of parasite maturation (22).

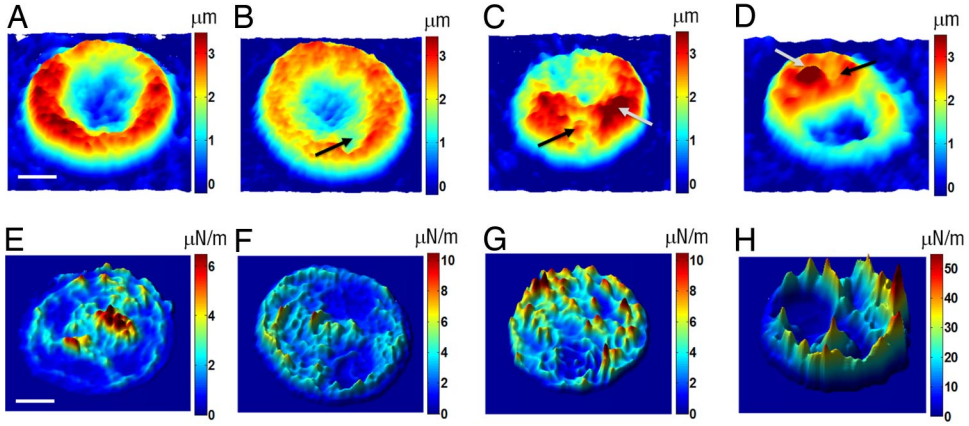

Fig. 3. Topographic images and effective elastic constant maps of *Pf*-RBCs. (*A* and *E*) Healthy RBC. (*B* and *F*) Ring stage. (*C* and *G*) Trophozoite stage. (*D* and *H*) Schizont stage. The topographic images in *A–D* are the instant thickness map of *Pf*-RBCs. The effective elastic constant maps were calculated from the root-mean-squared displacement of the thermal membrane fluctuations in the *Pf*-RBC membranes. Black arrows indicate the location of *P. falciparum*, and the gray arrows the location of hemozoin. (Bright-field and fluorescence micrographs provide information on locations of parasite and hemozoin; see *SI Text*). (Scale bar, 1.5 μm.)

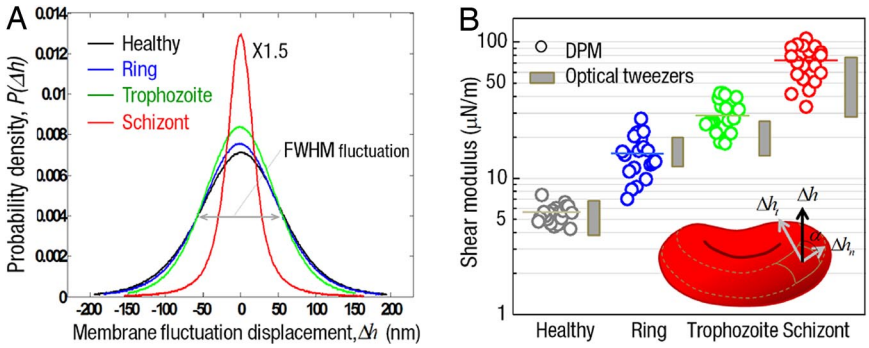

Fig. 4. Membrane fluctuations and in-plane shear modulus at different intraerythrocytic stages of *Pf*-RBCs. (*A*) Histograms of cell-thickness fluctuation of *Pf*-RBCs. (Histogram of the schizont stage is scaled down by a factor of 1.5.) (*B*) In-plane shear modulus of the RBC membrane versus developmental stage of *Pf*-RBCs. The in-plane shear modulus was calculated from the in-plane membrane displacement, Δh_n over the rims of RBCs. Also shown for comparison are the estimated from optical tweezers (22). (*Inset*) Illustration of RBC and membrane fluctuations: Δh, thickness fluctuations measured by DPM; Δh_t, in-plane membrane displacement; Δh_n, out-of-plane membrane displacement, and α, the angle between Δh and Δh_t. The measurements were performed at the room temperature (23°C) and for each group 20 samples were tested.

Effects of Temperature on Deformability of *Pf*-RBC During All Intraerythrocytic Stages. The effect of febrile temperature exposure on deformability of *Pf*-RBCs was evaluated at each parasite stage. Measurements were made at physiological temperature (37°C), febrile temperature (41°C), and physiological temperature after 45 min exposure at 41°C (one fever cycle) by using DPM. The results of these tests are summarized in Fig. 5 (membrane fluctuation) and Fig. 6 (in-plane shear modulus). The measured membrane in-plane shear modulus values reflect the overall cell deformability. The in-plane shear modulus for healthy RBCs are 6.2 ± 1.4, 4.9 ± 1.1, and 5.9 ± 1.0 μN/m, respectively, for 37°C, 41°C, and 37°C after one fever cycle. For ring stage, 14.5 ± 3.8, 20.4 ± 7.2, and 13.5 ± 4.2 μN/m; for trophozoite stage, 35.0 ± 9.0, 56.6 ± 14.9, and 46.7 ± 13.4 μN/m; and for schizont stage, 71.8 ± 21.0, 95.0 ± 25.5, and 99.6 ± 21.6 μN/m, respectively. Previous work consistently reports a shear modulus of 4–8 μN/m for healthy RBCs at physiological and febrile temperature (14). A higher shear modulus indicates a loss in deformability. As a control, healthy RBCs were evaluated at all three temperature conditions (Figs. 5*A* and 6*A*).

Results from testing ring stage display a marked decrease in deformability at febrile temperature compared with physiological temperature (Figs. 5*B* and 6*B*). On returning to physiological temperature, the deformability of ring stage returned to the level observed before the fever episode. Similar to ring stage, measured shear modulus values for trophozoite and schizont stage increase at febrile temperature compared with physiological temperature. However, measurements at physiological temperature after one fever cycle indicate permanent changes to deformability as a result of fever conditions. In trophozoites, a partial recovery of deformability was observed after returning to physiological temperature (Fig. 6*C*). Only half of the loss in deformability associated with a fever episode was recovered at the trophozoite stage. For schizont stage, essentially all loss of deformability as a result of febrile temperature exposure was permanent and was not recovered after fever conditions end (Fig. 6*D*).

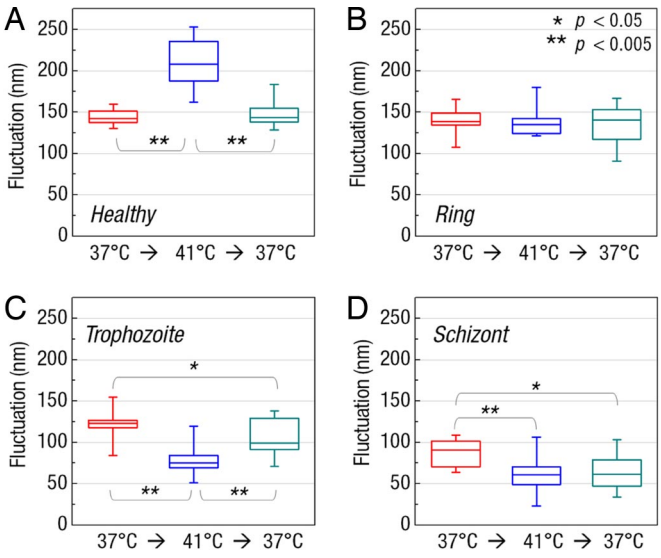

Fig. 5. Membrane fluctuations of *Pf*-RBCs at different temperatures. Membrane fluctuation at different parasitic development stages at 37°C, 41°C, and 37°C after one fever cycle for healthy RBCs (*A*), ring stage (*B*), trophozoite stage (*C*), and schizont stage of *Pf*-RBCs (*D*). The values for fluctuations are FWHM of the membrane fluctuation histograms. Graphs show the median (central horizontal line), standard deviations (box), and minimum and maximum values (vertical lines). For each group 15 samples were tested.

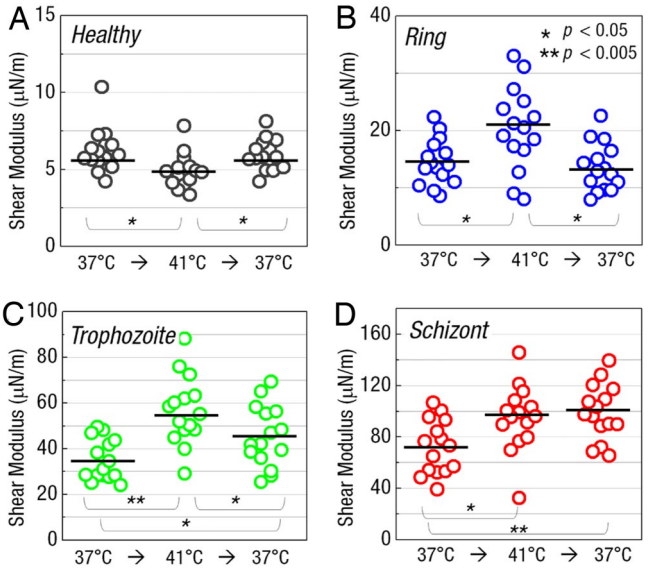

Fig. 6. In-plane shear modulus of *Pf*-RBCs at different temperatures. In-plane shear modulus at different parasitic development stages at 37°C, 41°C, and 37°C after one fever cycle for healthy RBCs (*A*), ring stage (*B*), trophozoite stage (*C*), and schizont stage (*D*). Symbols indicate individual *Pf*-RBCs. For each group 15 samples were tested.

Discussion

With *P. falciparum* parasitic development into the schizont stage, the normal discocyte shape is lost. Parasite modifications to the internal and membrane structure of invaded RBCs are implicated in the observed morphological changes (Fig. 3 *A–D*). Membrane stiffness also increases progressively with parasite development. In particular, the spatially averaged effective stiffness, $\langle k_e(x,y)\rangle$, at the schizont stage is up to an order of magnitude higher than that for healthy RBCs (Fig. 3 *E–H*). These results indicate that parasite development stage directly correlates with the amplitude of membrane fluctuations, and that the distribution of membrane fluctuations becomes much sharper with parasite development.

Interestingly, there is significant increase in membrane fluctuations [53% in the full-width half maximum (FWHM) value of the fluctuation displacement histogram] from physiological to febrile temperature ($P < 0.01$), which is only a 7.5% increase in absolute temperature. Evidently, such enhancement in the fluctuation cannot be explained simply by equilibrium thermodynamics alone, that is, by the increase in the Boltzmann factor k_BT. The substantial increase in membrane fluctuations indicates that RBC phospholipid membrane and spectrin network undergo structural changes that alter elastic properties, which is reflected in changes to membrane in-plane shear modulus, G (Fig. 4). One possible explanation is that a transitional structural change in spectrin molecular architecture occurs between physiological and febrile temperature, causing altered and reorganized cytoskeleton network. Both α- and β-spectrin molecules have a significant structural transition near 40°C (23). It has been shown that membrane shear modulus of healthy RBCs decreases by ≈20% when the temperature increases from 23 to 41°C (21). From physiological to febrile temperature, membrane fluctuations decrease significantly ($P < 0.01$) for all infected test conditions (Fig. 3), with trophozoite and schizont stages showing the strongest temperature dependence. Based on comparison with results from healthy RBC and associated changes of in-plane shear modulus (Fig. 4*B*), we postulate that intraerythrocytic parasite development causes an opposite effect. Parasite-exported proteins that target RBC membrane can alter thermally induced spectrin-folding transitions involved in stabilizing erythrocyte cytoskeleton (24). Expression of *P. falciparum* genes is known to be affected by exposure to 41°C (25). Under febrile conditions, increased levels of parasite-exported proteins could contribute to large changes in membrane fluctuations observed by DPM between physiological and febrile temperatures. One example is the ring-infected erythrocyte surface antigen (RESA). When RESA binds to spectrin, normal balance between spectrin dimers and tetramers in the cytoskeletal network is skewed toward tetramer formation, which results in increased membrane stability (26). As a result, RESA enhances RBC resistance to mechanical and thermal damage. Moreover, elevated thermal stability conferred by RESA plays a protective role for *Pf*-RBCs against damage at febrile temperature (27). The possible specific role of other membrane proteins and histidine-rich proteins in influencing thermal and mechanical stability of RBCs over the temperature range of interest is presently not fully understood. The development of adhesion properties at the trophozoite and schizont stages can also contribute to significant decrease in fluctuation observed by DPM at these stages, especially at febrile temperature. For the same febrile temperature, our results indicate that fluctuation amplitude progressively decreases as a parasite matures from the ring to the schizont stage.

The findings presented in Figs. 5 and 6 reveal that effects of fever episodes cause irreversible changes to deformability of *Pf*-RBCs. These experiments mimic *in vivo* conditions that *Pf*-RBCs experience and provide information that cannot be extracted from mechanical experiments performed at a constant temperature. Plastic behavior caused by a febrile episode is not observed at the ring stage. Decreased deformability observed under febrile conditions is recovered on returning to physiological temperature. The decrease in deformability of *Pf*-RBCs may be attributed to exported parasite proteins that interact with the host RBC membrane. The ability of ring stage to regain deformability could play an important role in their ability to avoid splenic clearance when circulating. Trophozoite and schizont stages display significant plastic changes to deformability. Again, decreased deformability for mature stages may be also attributed largely to parasite-exported proteins that associate with the membrane. Parasite protein exportation is likely accelerated by thermal energy. In turn, febrile episodes may be accelerating parasite protein exportation to the membrane that results in advancing the loss of deformability. Both reduced deformability and the development of adhesion properties contribute to sequestration of trophozoite and schizont stage. The temperature-related permanent loss of deformability found in our experiments is greater than anticipated and can be viewed as an additional driving force to impede microcirculation and promote sequestration. The plastic behavior of trophozoite and schizont stages in response to fever could also have implications when treatments are used to suppress fever episodes. Additional studies would be needed to explore this possibility.

Finally, the optical experimental techniques (TPM and DPM) used to measure the refractive index maps and the membrane fluctuations in this study offer unique advantages over other more commonly used techniques, such as micropipette aspiration, optical tweezers, laminar shear flow, and magnetic twisting cytometry. TPM quantitatively and noninvasively measures the three-dimensional maps of refractive index, which provides a measure of Hb content of single *Pf*-RBCs. Indeed, TPM does not require any special sample preparation because the refractive index is an intrinsic optical property. DPM is able to measure nanometer level membrane fluctuations without any direct, and potentially invasive, contact with a cell. The optical layout of DPM is such that the sample temperature can be regulated easily without affecting of the rest of the apparatus, a common limitation of other techniques. In addition, deformability of living cells, measured by thermally driven membrane fluctuations, ensures mechanical properties in the linear regime. Also, measurements are made within seconds once a specific cell is identified. Thus, the technique provides the flexibility to experiment on a large number of samples under a variety of well controlled test conditions in a reasonable time span.

Conclusions

We have presented three-dimensional maps of refractive index of *Pf*-RBCs during all intererythrocytic stages, from which we determine the Hb concentration of *Pf*-RBCs. We have also presented systematic measurements of nanoscale fluctuations associated with RBCs parasitized at all stages by *P. falciparum* at physiological and febrile temperatures. Our approach to studying *Pf*-RBCs uniquely combines optical interferometry, biophysics, and cell nanomechanics. A method has been presented to extract elastic properties from membrane fluctuation results, and this technique is validated by quantitative comparisons of elastic moduli of RBCs over all parasite maturation stages with prior, independent experimental data obtained with laser tweezers (14, 22). Compared with other techniques for assessing RBC mechanical properties, such as electric field deformation, micropipette aspiration, optical tweezers, and magnetic bead excitation, the method presented here has distinct advantages of being spatially resolved and noncontact. We envision that this methodology could offer potentially powerful means to link cell membrane fluctuations with pathological conditions that lead to human disease states by providing quantitative information that could not be extracted through other experimental techniques.

These results point to major new avenues for exploiting membrane fluctuations as quantitative indicators of the onset and progression of pathological states that could lead to diseases. In addition, the information provided by diffraction phase microscopy can guide theory and computational simulations that address a

broader range of cell biology problems concerning human health, disease diagnostics, therapeutics, and drug efficacy assays.

Materials and Methods

Preparation of *Pf*-RBCs and Parasite Culture. *P. falciparum* 3D7A were maintained in leukocyte-free human O+ erythrocytes (Research Blood Components) under an atmosphere of 3% O_2, 5% CO_2, and 92% N_2 in RPMI medium 1640 (Gibco Life Technologies) supplemented with 25 mM Hepes (Sigma), 200 mM hypoxanthine (Sigma), 0.209% $NaHCO_3$ (Sigma), and 0.25% albumax I (Gibco Life Technologies). Cultures were synchronized successively by concentration of mature schizonts by using plasmagel flotation (28) and sorbitol lysis 2 h after merozoite invasion to remove residual schizonts (29).

Measurements were performed at 14–20 h (ring stage), 20–36 h (trophozoite stage), and 36–48 h (schizont stage) after merozoite invasion. To identify the infected RBCs, we treated the parasites with DAPI staining. Before the DPM dynamic measurements, we recorded epi-fluorescence images, as described in ref. 19.

Healthy RBC control samples and *Pf*-RBCs samples were diluted in PBS to $\approx 10^6$ RBC per ml before membrane fluctuation experiments. Both healthy and *Pf*-RBCs adhere to the glass substrate rapidly and strongly. However, adhesion of the bottom membrane of RBCs does not significantly affect to the fluctuation of the upper membrane. DPM measurement shows no significant difference in membrane fluctuation between RBCs positioned on the glass substrate and RBCs firmly attached to the glass substrate by using poly-L-lysine followed the protocol indicated in ref. 30.

Diffraction Phase Microscopy. An Ar^{2+} laser ($\lambda = 514$ nm) was used as illumination source for an inverted microscope (IX71, Olympus). The microscope was equipped with a 40× objective (0.65 N.A.), which facilitates a diffraction-limited transverse resolution of 400 nm. With the additional relay optics used outside the microscope, the overall magnification of the system was ≈200×. EMCCD (Photonmax 512B, Princeton Instruments) was used to image interferogram. DPM employs the principle of laser interferometry in a common path geometry and thus provides full-field quantitative phase images of RBCs with unprecedented optical pathlength stability (19). The instantaneous cell thickness map is obtained as $h(x, y, t) = \lambda/2\pi\Delta n\ \varphi(x, y, t)$, with φ the quantitative phase image measured by DPM. The refractive index contrast Δn between the RBC and the surrounding PBS is mainly contributed to the Hb, which is optically homogeneous in cytosol. We used tomographic phase microscopy (TPM) to retrieve three-dimensional refractive index for all of the stages of *Pf*-RBCs and healthy RBCs. The DPM optical pathlength stability is 2.4 mrad, which corresponds to a membrane displacement of 3.3 nm (19).

Tomographic Phase Microscopy. Tomographic phase microscopy (TPM) is a technique that can map the three-dimensional distribution of refractive index in live cells and tissues (16). In TPM, the sample-induced optical phase shift is imaged by using a phase-shifting heterodyne interferometer. Phase images are recorded by varying the directions of illumination. The angle of illumination ranges from −60 to 60° and angular step is 0.2°. It takes ≈10 s to scan the entire angular range. Phase image at each step of angle corresponds to angular projection of refractive index at the illumination angle. The custom built microscopy and CMOS camera (FASTCAM 1024 PCI, Photron) are used to measure interferograms. With the set of angular projection phase images, a filtered back-projection algorithm is used to calculate a three-dimensional refractive index. The transverse and axial resolutions are 0.3 and 0.6 μm, respectively, and the accuracy of index measurement is 0.001.

Temperature Control. The microscopic stage was equipped with a temperature controller (TC-202A, Warner Instruments), which uses a thermistor to set the temperature of the sample to within ±0.2°C. The well containing RBCs was placed in contact with the controller chamber, such that heat transfer and thermal equilibrium between the two systems were attained relatively fast, after 3–4 min. However, we measured the individual RBC at multiple temperature points by waiting ≈10 min for each new temperature, which ensured thermal equilibrium.

Statistical Analysis. *P* values were calculated by two-tailed Mann–Whitney rank sum tests comparing the FWHM fluctuations and shear modulus values between various test conditions. All of the numbers following the ± sign in the text are standard deviations.

ACKNOWLEDGMENTS. We thank K. Badizadegan, R. R. Dasari, and M. Dao for technical discussions, J. P. Mills for helpful suggestions on experimental design and data analysis, and Malaria Research and Reference Reagent Resource, American Type Culture Collection, for providing us with 3D7A parasite. This work was supported by National Institutes of Health Grants P41-RR02594-18 and(1-R01-GM076689-01, National Science Foundation Grant DBI-0754339, and the Interdisciplinary Research Group on Infectious Diseases, which is funded by the Singapore-MIT Alliance for Research and Technology Center. Y.P. was supported by Cambridge Foundation Fellowship, Samsung Scholarship, and Whitaker Health Science Fellowship. M.D.-S. and G.L. were partially supported by Global Enterprise for MicroMechanics and Molecular Medicine (GEM4) postdoctoral fellowships.

1. Kilejian A (1979) Characterization of a protein correlated with the production of knob-like protrusions on membranes of erythrocytes infected with *Plasmodium falciparum*. *Proc Natl Acad Sci USA* 76:4650–4653.
2. Sherman IW (1979) Biochemistry of Plasmodium (malarial parasites). *Microbiol Rev* 43(4):453.
3. Goldberg DE, Slater AFG, Cerami A, Henderson GB (1990) Hemoglobin degradation in the malaria parasite *Plasmodium falciparum*: An ordered process in a unique organelle. *Proc Natl Acad Sci USA* 87:2931–2935.
4. Nash GB, O'Brien E, Gordon-Smith EC, Dormandy JA (1989) Abnormalities in the mechanical properties of red blood cells caused by Plasmodium falciparum. *Blood* 74(2):855–861.
5. Cranston HA, *et al.* (1984) Plasmodium falciparum maturation abolishes physiologic red cell deformability. *Science* 223(4634):400–403.
6. Paulitschke M, Nash GB (1993) Membrane rigidity of red blood cells parasitized by different strains of Plasmodium falciparum. *J Lab Clin Med* 122(5):581–589.
7. Miller LH, Baruch DI, Marsh K, Doumbo OK (2002) The pathogenic basis of malaria. *Nature* 415(6872):673–679.
8. Discher DE, Mohandas N, Evans EA (1994) Molecular maps of red cell deformation: Hidden elasticity and in situ connectivity. *Science* 266(5187):1032.
9. Gov NS, Safran SA (2005) Red blood cell membrane fluctuations and shape controlled by ATP-induced cytoskeletal defects. *Biophys J* 88(3):1859.
10. Lawrence CLL, Gov N, Brown FLH (2006) Nonequilibrium membrane fluctuations driven by active proteins. *J Chem Phys* 124:074903.
11. Tuvia S, Levin S, Bitler A, Korenstein R (1998) Mechanical fluctuations of the membrane-skeleton are dependent on F-actin ATPase in human erythrocytes. *J Cell Biol* 141(7):1551–1561.
12. Li J, Dao M, Lim CT, Suresh S (2005) Spectrin-level modeling of the cytoskeleton and optical tweezers stretching of the erythrocyte. *Biophys J* 88(5):3707–3719.
13. Glenister FK, Coppel RL, Cowman AF, Mohandas N, Cooke BM (2002) Contribution of parasite proteins to altered mechanical properties of malaria-infected red blood cells. *Blood* 99(3):1060–1063.
14. Mills JP, *et al.* (2007) Effect of plasmodial RESA protein on deformability of human red blood cells harboring *Plasmodium falciparum Proc Natl Acad Sci USA* 104:9213–9217.
15. Kwiatkowski D (1989) Febrile temperatures can synchronize the growth of Plasmodium falciparum in vitro. *J Exp Med* 169(1):357–361.
16. Choi W, *et al.* (2007) Tomographic phase microscopy. *Nat Methods* 4:717–719.
17. Tilley L, McFadden G, Cowman A, Klonis N (2007) Illuminating *Plasmodium falciparum*-infected red blood cells. *Trends Parasitol* 23:268–277.
18. Friebel M, Meinke M (2006) Model function to calculate the refractive index of native hemoglobin in the wavelength range of 250–1100 nm dependent on concentration. *Appl Opt* 45(12):2838–2842.
19. Park YK, Popescu G, Badizadegan K, Dasari RR, Feld MS (2006) Diffraction phase and fluorescence microscopy. *Opt Exp* 14(18):8263–8268.
20. Lee JCM, Discher DE (2001) Deformation-enhanced fluctuations in the red cell skeleton with theoretical relations to elasticity, connectivity, and spectrin unfolding. *Biophys J* 81(6):3178–3192.
21. Waugh R, Evans EA (1979) Thermoelasticity of red blood cell membrane. *Biophys J* 26(1):115–131.
22. Suresh S, *et al.* (2005) Connections between single-cell biomechanics and human disease states: Gastrointestinal cancer and malaria. *Acta Biomater* 1(1):15–30.
23. Minetti M, Ceccarini M, Di Stasi AMM, Petrucci TC, Marchesi VT (1986) Spectrin involvement in a 40°C structural transition of the red blood cell membrane. *J Cell Biochem* 30:361–370.
24. Da Silva E, *et al.* (1994) The *Plasmodium falciparum* protein RESA interacts with the erythrocyte cytoskeleton and modifies erythrocyte thermal stability. *Mol Biochem Parasitol* 66(1):59–69.
25. Oakley MSM, *et al.* (2007) Molecular factors and biochemical pathways induced by febrile temperature in intraerythrocytic *Plasmodium falciparum* parasites. *Infect Immun* 75(4):2012–2025.
26. Pei X, *et al.* (2007) The ring-infected erythrocyte surface antigen (RESA) of. *Plasmodium falciparum* stabilizes spectrin tetramers and suppresses further invasion. *Blood* 110(3):1036–1042.
27. Silva MD, *et al.* (2005) A role for the. *Plasmodium falciparum* RESA protein in resistance against heat shock demonstrated using gene disruption. *Mol Microbiol* 56(4):990–1003.
28. Pasvol G, Wilson RJ, Smalley ME, Brown J (1978) Separation of viable schizont-infected red cells of. *Plasmodium falciparum* from human blood. *Ann Trop Med Parasitol* 72(1):87–88.
29. Lambros C, Vanderberg JP (1979) Synchronization of. *Plasmodium falciparum* erythrocytic stages in culture. *J Parasitol* 65(3):418–420.
30. Hategan A, Sengupta K, Kahn S, Sackmann E, Discher DE (2004) Topographical pattern dynamics in passive adhesion of cell membranes. *Biophys J* 87(5):3547–3560.

Supporting Information

Park *et al.* 10.1073/pnas.0806100105

SI Text

Identifying the Infected RBCs. To identify *Plasmodium falciparum* infected RBCs, we used both bright-field and fluorescence microscopy (Fig. S1). Fig. S1 *A–D* show bright-field images of healthy RBC, ring stage, trophozoite, and schizont. To distinguish schizont from trophozoite stages, we used the DAPI staining and fluorescent microscopy as in Fig. S1 *E* and *F*.

Masking the Parasite. Because *P. falciparum* parasites have a different refractive index from the RBC hemoglobin solution, the movement of *P. falciparum* could cause artifacts in quantifying the motion of RBC membrane. To minimize this effect, we used the masks for the region where the parasite is located and excluded those areas from the calculation of the mean squared displacements for analyzing the membrane dynamics. The procedure to generate the masks is illustrated in Fig. S2. First, we identified the shape and size of a RBC by using bright-field microscopy (Fig. S2*A*) and made a mask for the outer shape of the cell (Fig. S2*B*). Fluorescent microscopy provided the information about the location of *P. falciparum* parasite (Fig. S2*C*). From this information we generated the mask for the parasite. By subtracting the mask for the parasite (Fig. S2*D*) from the mask for the RBC, we were able to identify the mask for the parasite-free region (Fig. S2*E*). Additional smooth filters were used to minimize the artifacts coming from the shape edge.

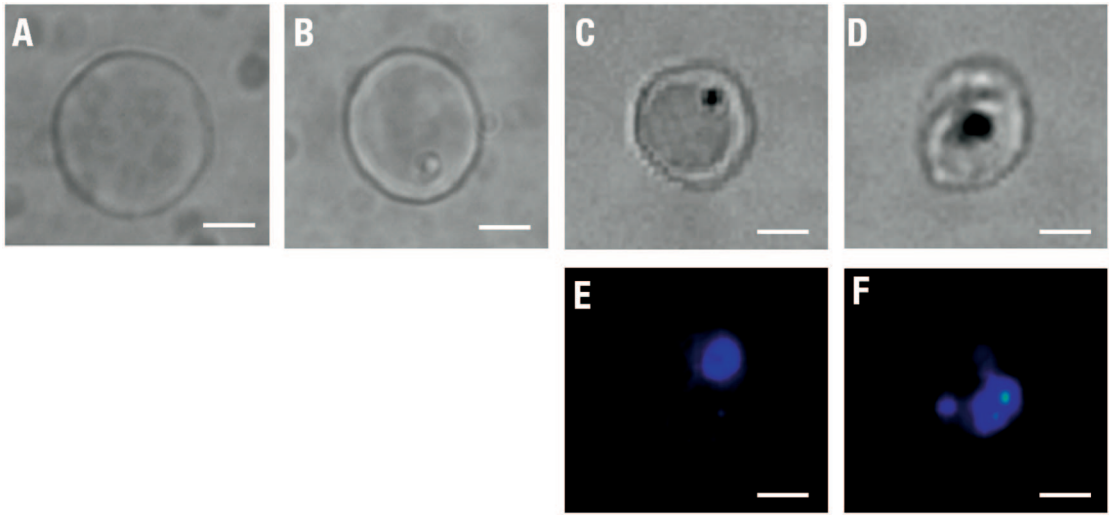

Fig. S1. Identifying the infected RBCs by fluorescence. (*A–D*) Bright-field images. (*E* and *F*) DAPI stained fluorescent images. (*A*) Healthy RBC, (*B*) ring stage, (*C* and *E*) trophozoite stage, and (*D* and *F*) Schizont stage. (Scale bar, 1.5 μm.)

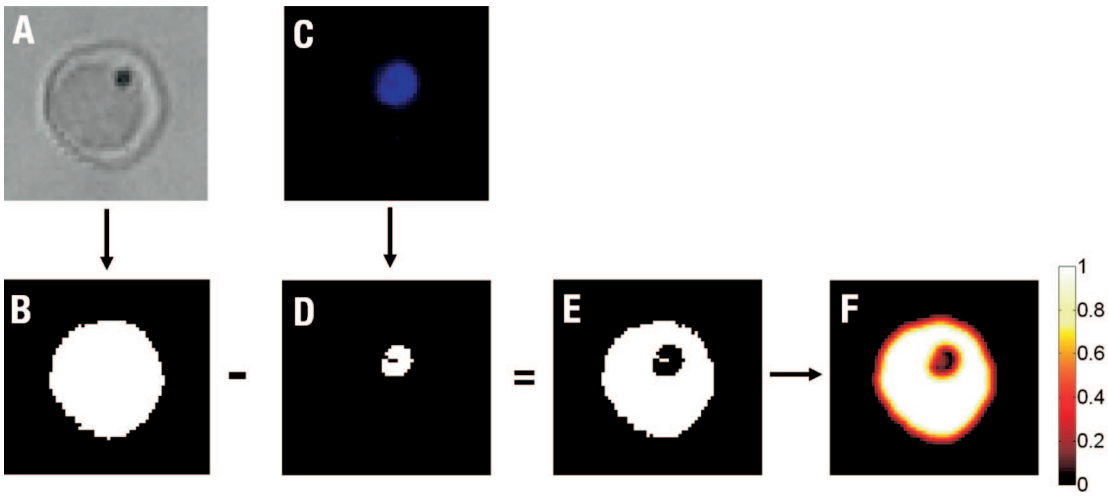

Fig. S2. Masking the parasite in the PDM image. (*A*) Bright-field image. (*B*) Mask from the bright-field image. (*C*) Fluorescent image. (*D*) Mask from the fluorescent image. (*E*) Subtraction of *D* from *B*. (*F*) Mask after smooth filter was applied on *E*.

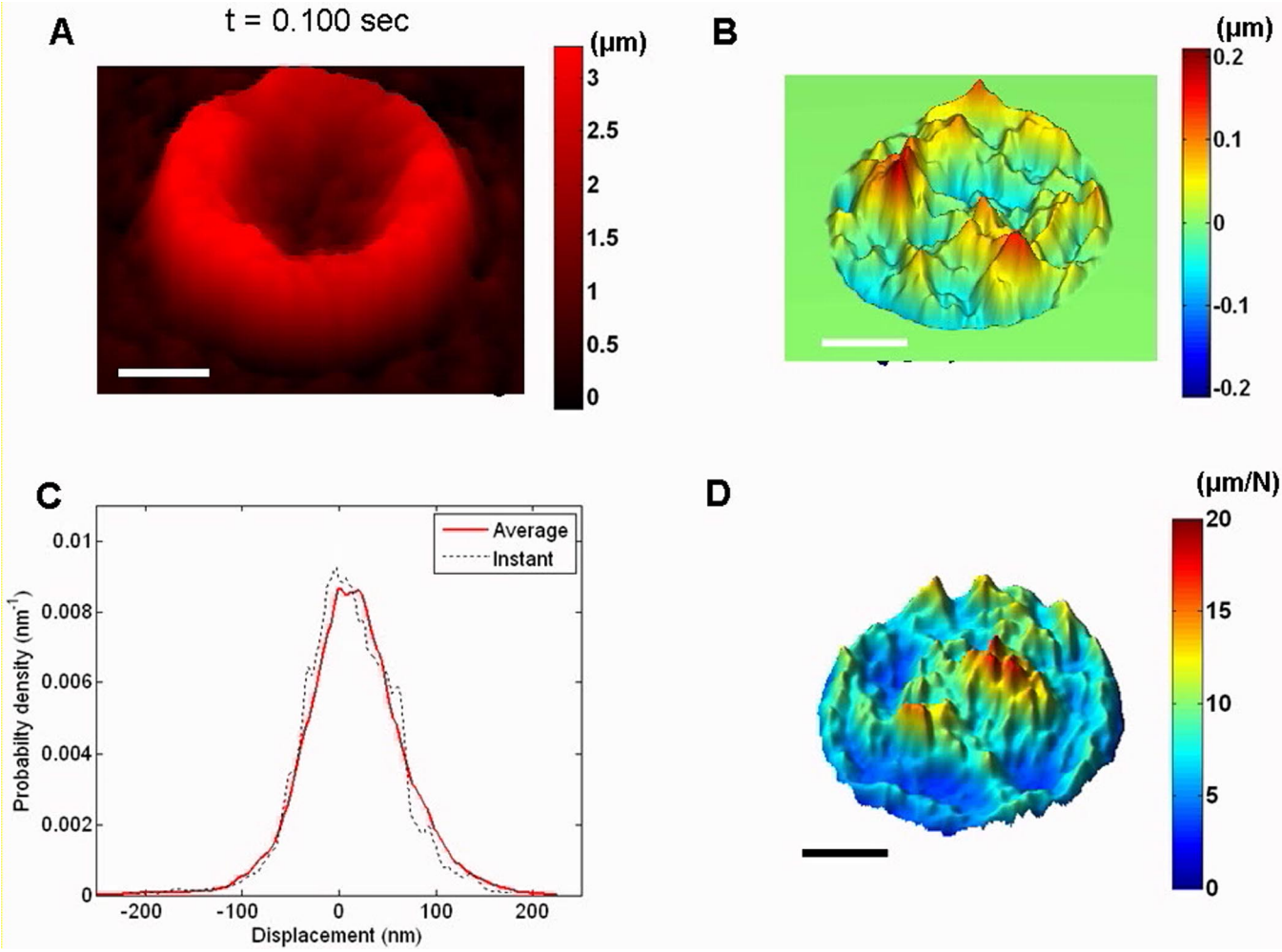

Movie S1. Movie clip of membrane fluctuations of the healthy RBC. (*A*) Topographic information measured by DPM. (*B*) Displacement subtracted from every consequence frame. (*C*) Histogram of displacement. (*D*) Effective spring constant k_e.

Movie S1 (AVI)

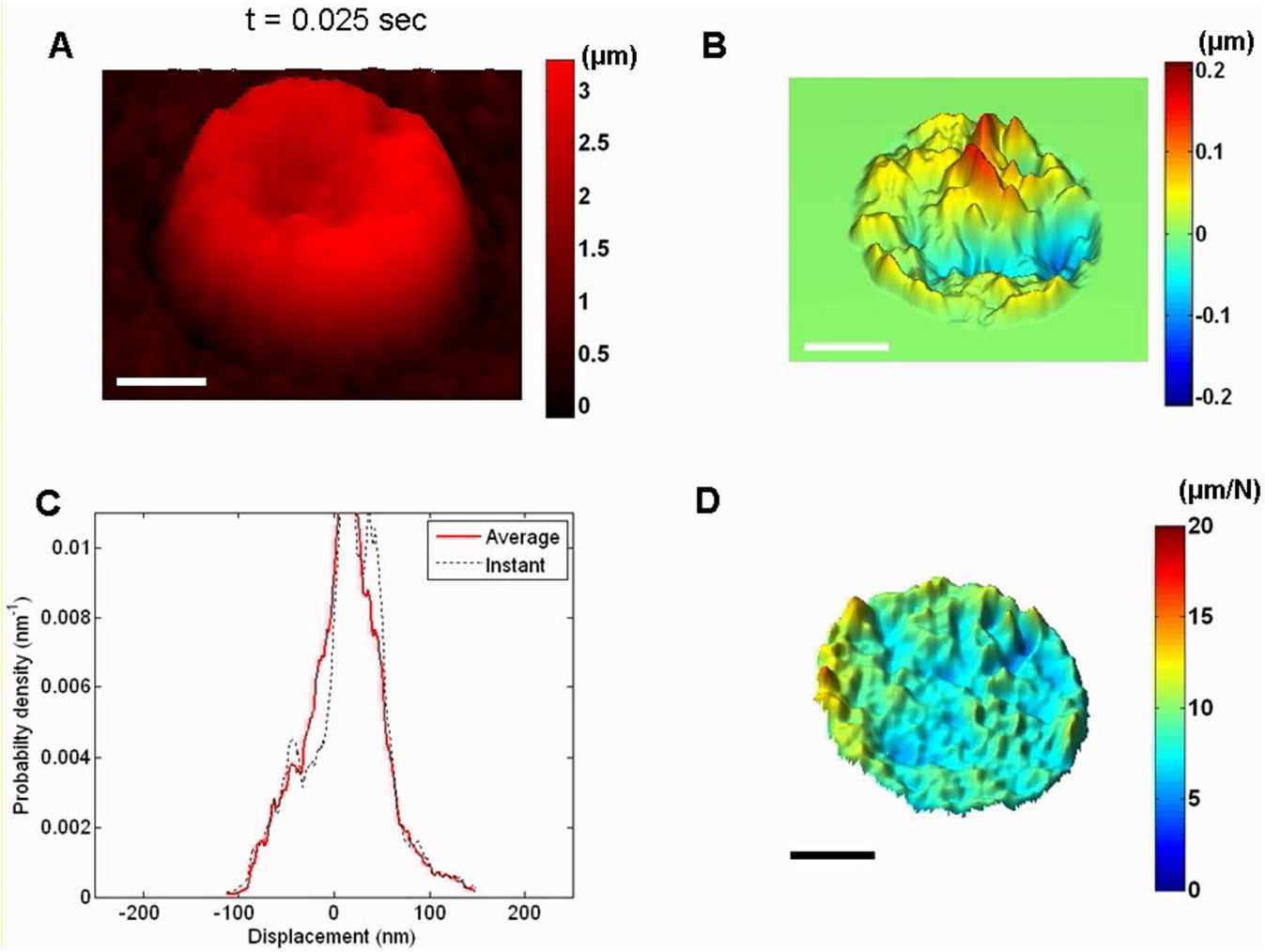

Movie S2. Movie clip of membrane fluctuations of the ring stage of parasitization. (*A*) Topographic information measured by DPM. (*B*) Displacement subtracted from every consequence frame. (*C*) Histogram of displacement. (*D*) Effective spring constant k_e.

Movie S2 (AVI)

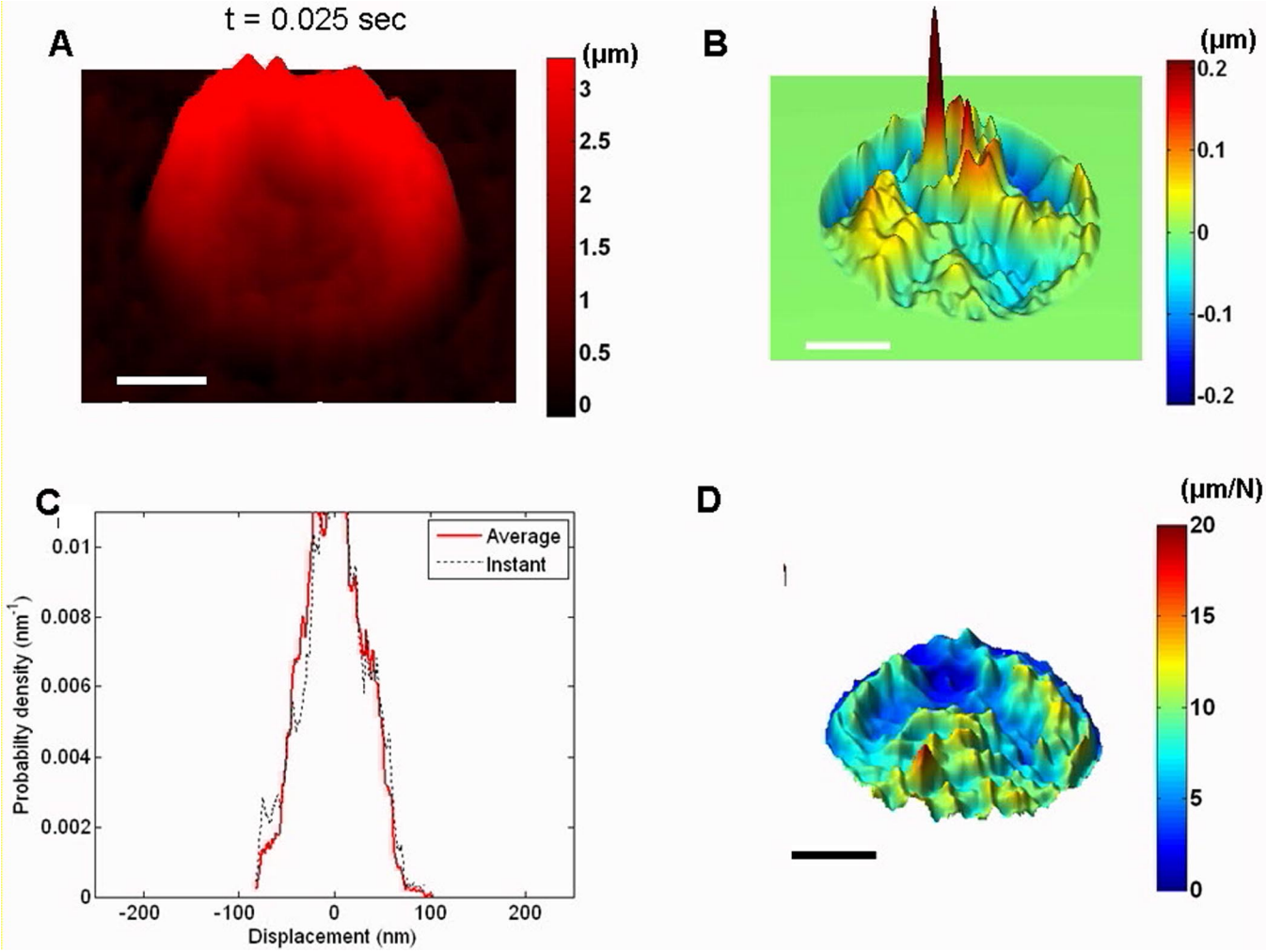

Movie S3. Movie clip of membrane fluctuations of the trophozoite stage of parasitization. (*A*) Topographic information measured by DPM. (*B*) Displacement subtracted from every consequence frame. (*C*) Histogram of displacement. (*D*) Effective spring constant k_e.

Movie S3 (AVI)

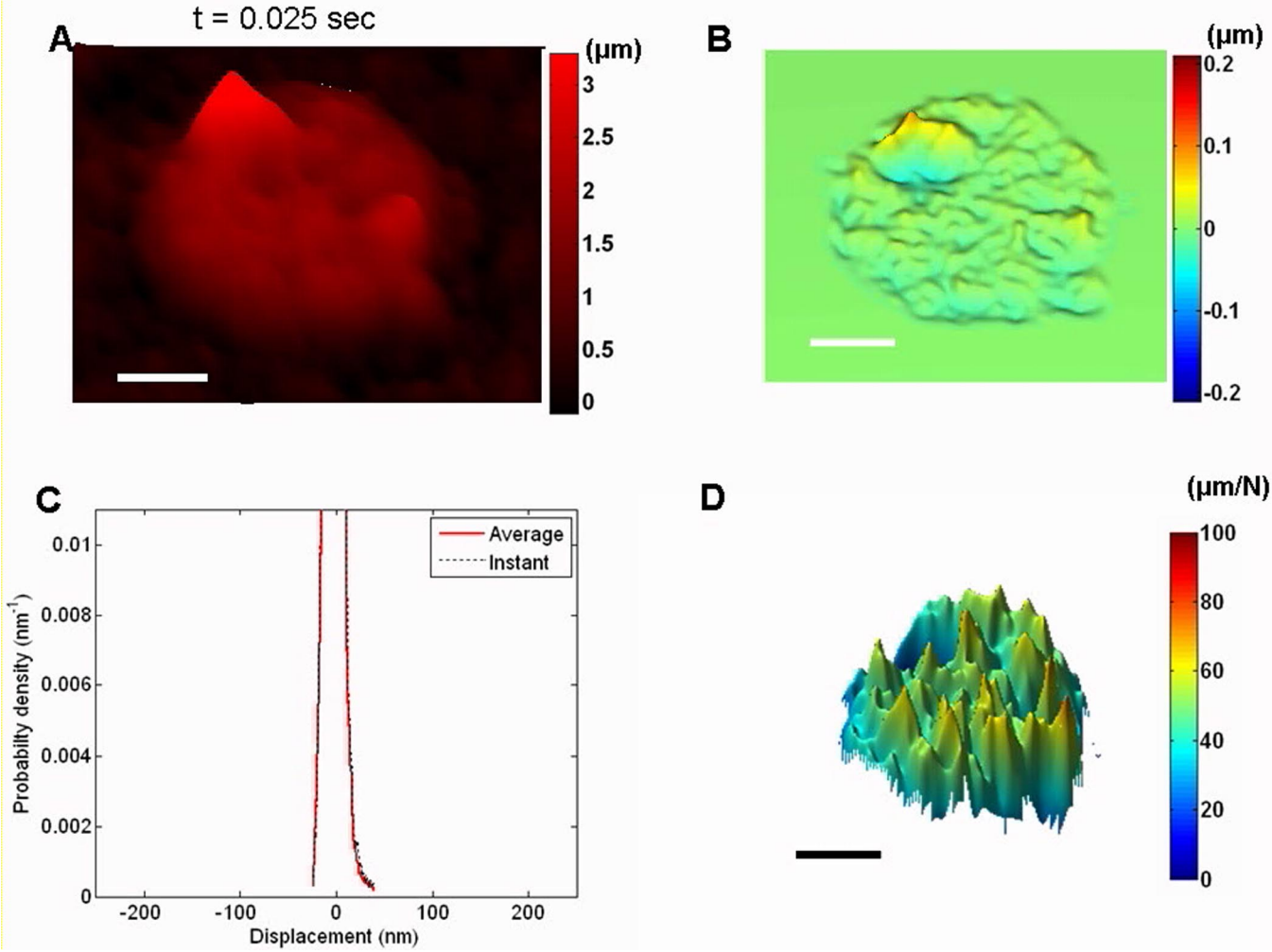

Movie S4. Movie clip of membrane fluctuations of the schizont stage of parasitization. (*A*) Topographic information measured by DPM. (*B*) Displacement subtracted from every consequence frame. (*C*) Histogram of displacement. (*D*) Effective spring constant k_e.

Movie S4 (AVI)